Supporting Information

Rational Design of Circularly Polarized Luminescence Active Chiral Metal-organic Frameworks for Logic Device

Hongrui Zheng[a], Qingqing Wang[a], Fei Wang*[a], Shangda Li*[a], and Jian Zhang*[a]

[a]State Key Laboratory of Structural Chemistry, Fujian Institute of Research on the Structure of Matter, the Chinese Academy of Sciences, Fuzhou, Fujian 350002, People's Republic of China; College of Chemistry, Fuzhou University, Fuzhou, Fujian 350108, People's Republic of China.
Email: wangfei04@fjirsm.ac.cn; sdli@fjirsm.ac.cn; zhj@fjirsm.ac.cn.

Contents

1. General Information

1.1 Materials.

All commercially available chemicals were purchased from the respective suppliers such as Adamas, Aladdin, Bide, and others. They are used as received without further purification. Homochiral ligands (L/D-H_2IDPA) were prepared using the optimized procedure previously reported by us.[1, 2]

1.2 Instruments.

Crystallographic Data Collection and Refinement.

The 6 single crystals were successively mounted and transferred to the goniometer head for indexing. A ROD, Synergy Custom system, HyPixs diffractometer equipped with a HyPix CCD detector and Cu Kα radiation (λ = 1.54184) Å) and Mo Kα radiation (λ= 0.71073) were used for data collection. The crystal was kept at 293K and 100K during data collection. The structure was solved using the intrinsic phasing SHELXT-2015 structure solution program within Olex2 and refined with the least-squares minimization SHELXL-2015 refinement package. The crystallographic data for **L-1**, **L-2**, **L-3** and **D-1**, **D-2**, **D-3** are presented in Tables S1and S2, respectively.

Physical measurements.

Powder X-ray diffraction (PXRD) patterns were obtained using Cu Kα radiation (λ = 1.54056 A) on the Rigaku Mini Flex Type II automatic diffraction system. At room temperature, measured in the 2θ range of 5 to 50°, the scan rate is 3°min^{-1}. The working power is 40kV, 30mA. Thermal gravimetric analysis (TGA) was performed on the STA 449F3 analyzer at heating rate of 10°C·min^{-1} under nitrogen atmosphere from 24 to 800°C. The Perkin Elmer Lamda-950 UV spectrophotometer uses $BaSO_4$ as the standard (100% reflectivity) to scan and record UV-VIS diffuse reflection data in the range of 200-800 nm at room temperature.

Photophysical and Chiroptical Properties

Photoluminescence (PL) spectra and lifetime data were collected on the FLS1000 spectrometer in Edinburgh. A multi-exponential decay function of $I(\tau)=A_1 \exp(-\tau/\tau_1) + A_2 \exp(-\tau/\tau_2) + \cdots + A_i \exp(-\tau/\tau_i)$ is used to fit the luminescence lifetime (τ) of a solid sample, where Ai and Ai exp represent the amplitude and lifetime of individuals component in the multi-exponential decay curve. The circular dichroic spectra of the samples were determined in a MOS-450 circular dichroic spectrometer using a KBr to sample ratio of 20:1 grinding pressure sheet. The circular polarization luminescence (CPL) of single crystal was measured by CPL-300 spectrometer. In the measurement wavelength range of 320~700nm, the crystal face of the measured crystal was determined to be 100 crystal faces, and the crystal size was 200 microns.

2. Experimental Section

2.1 Optical properties of ligands.

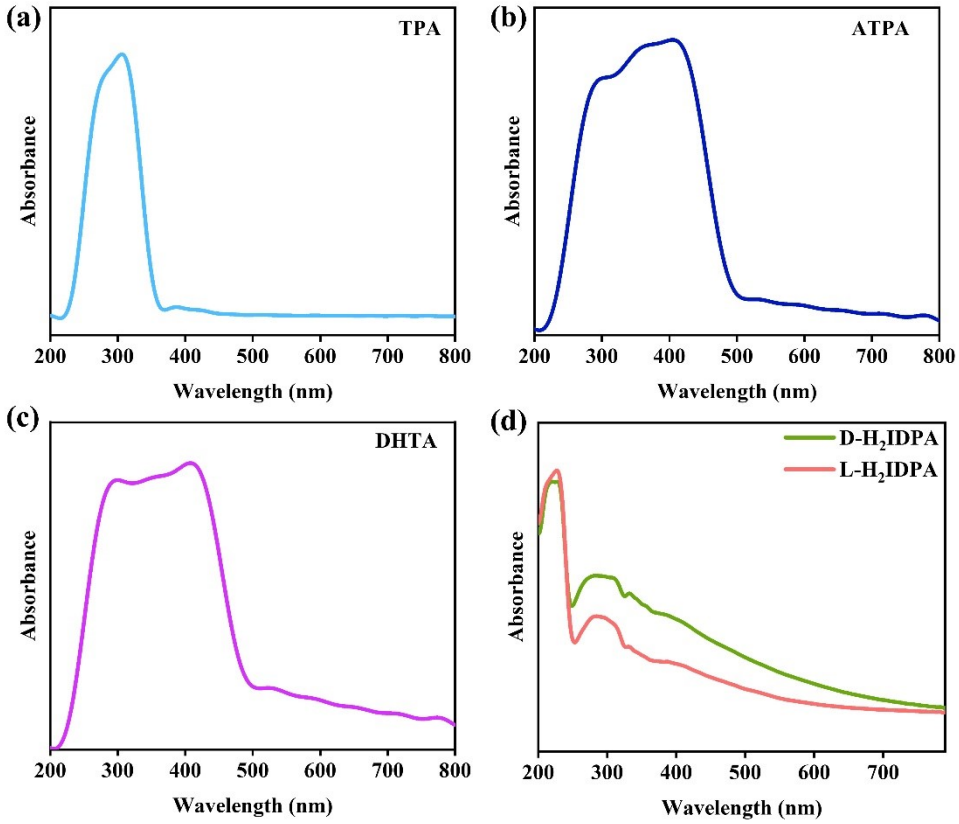

Figure S1. Ultraviolet absorption spectra of TPA (a), ATPA (b), DHTA (c) and L/D-H_2IDPA (d).

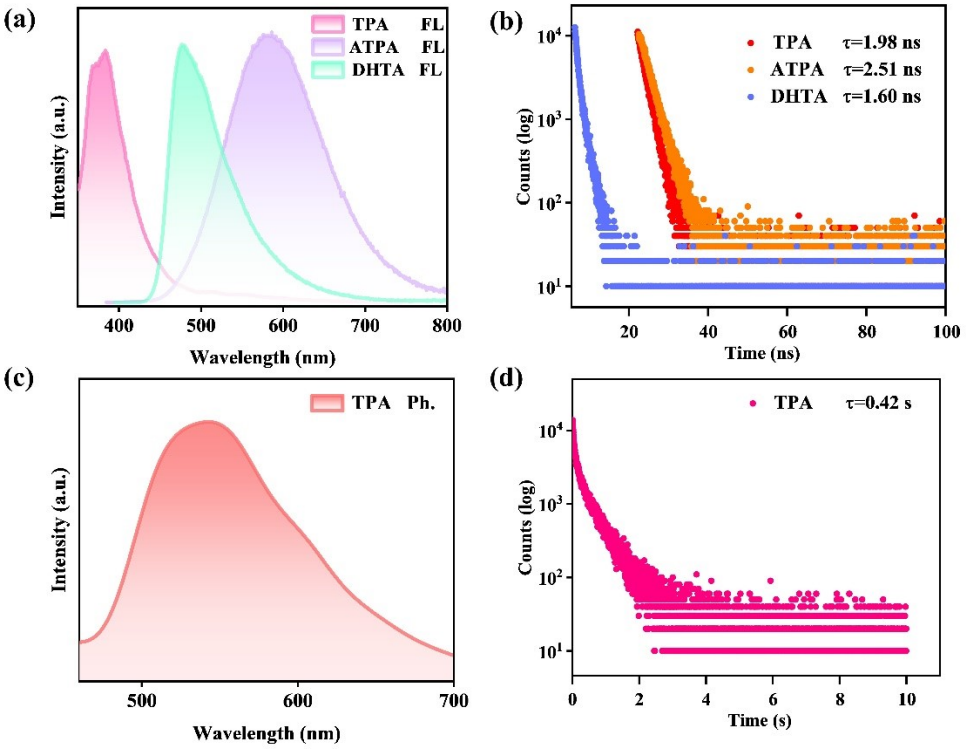

Figure S2. (a) fluorescence spectra of TPA, ATPA, and DHTA. (b) fluorescence lifetime spectra of TPA, ATPA, and DHTA. (c) phosphorescent spectra of TPA. (d) phosphorescent lifetime spectra of TPA.

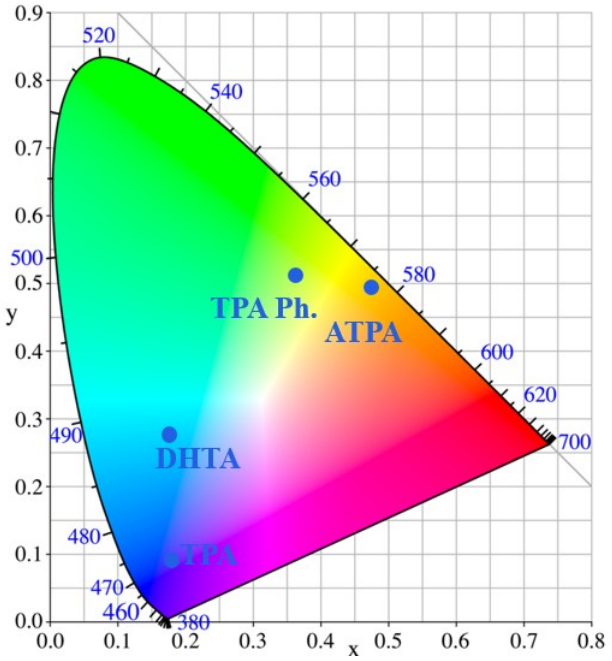

Figure S3. The CIE coordinates of TPA, ATPA and DHTA.

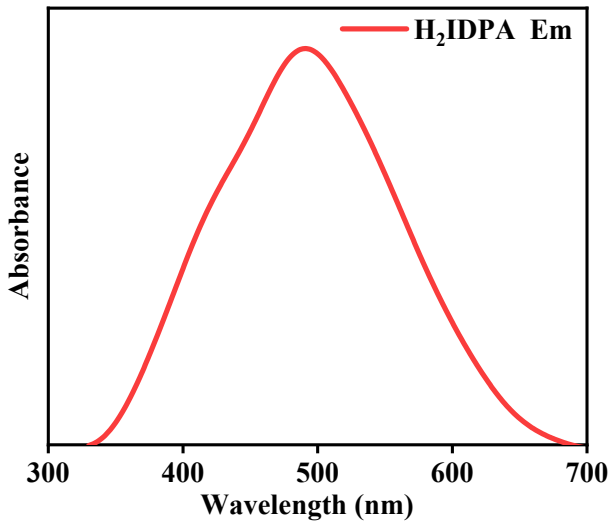

Figure S4. The fluorescence spectra of H_2IDPA.

2.2 Initial evaluation of the ligand combination using CPF-ET.

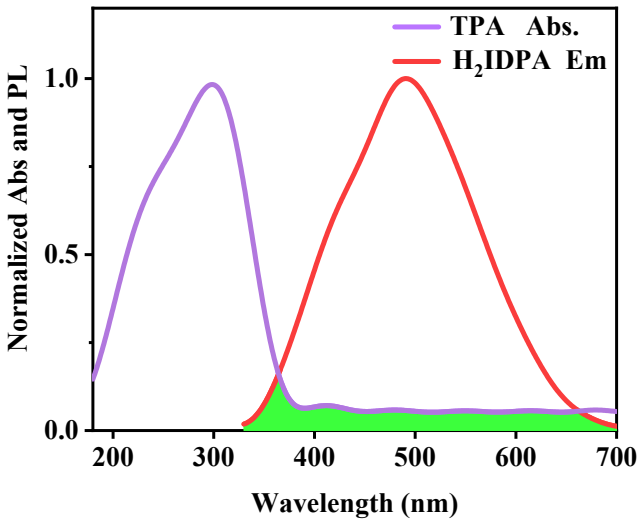

Figure S5. The ultraviolet absorption spectra of TPA and the fluorescence emission spectra of H_2IDPA.

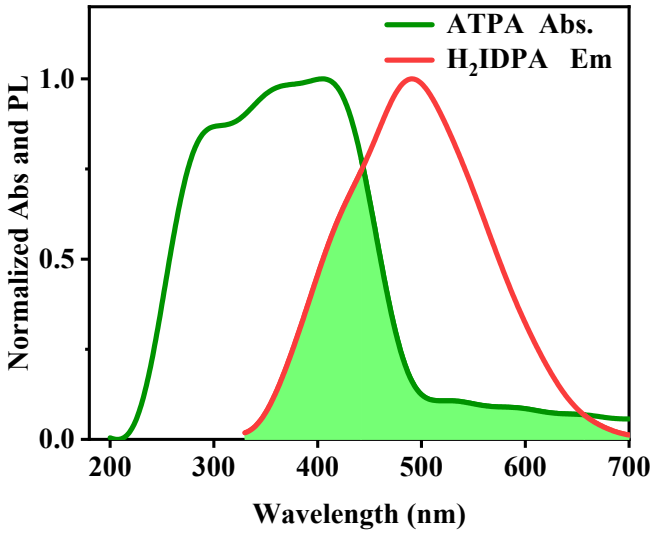

Figure S6. The ultraviolet absorption spectra of ATPA and the fluorescence emission spectra of H_2IDPA.

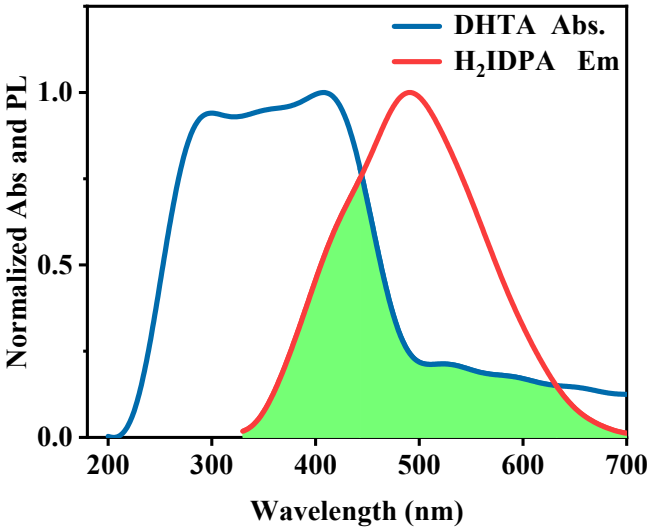

Figure S7. The ultraviolet absorption spectra of DHTA and the fluorescence emission spectra of H_2IDPA.

2.3 Synthesis of compounds

Preparation of [L-Zn_2(TPA) (H_2IDPA)$_2$] (L-1): 59.5 mg (0.2 mmol) of $Zn(NO_3)_2 \cdot 6H_2O$, 33.2 mg (0.2 mmol) of TPA, and 50 mg (0.23 mmol) of L-H_2IDPA were weighed into a 25-mL scintillation vial. To the solids, 3 mL of DMF, 1 mL of EtOH, and 500 μL of water were added. The resulting transparent solution was capped and heated in an oven at 120 °C for 2 days, followed by slow cooling. Colorless, bulk-like crystals were obtained and washed with DMF. Yield: 72%.

Preparation of [D-Zn_2(TPA) (H_2IDPA)$_2$] (D-1): Under the same conditions used for the preparation of **L-1**, D-H_2IDPA was substituted for L-H_2IDPA to obtain high-quality, colorless bulk crystals of **D-1**.

Preparation of [L-Zn_2(ATPA) (H_2IDPA)$_2$] (L-2): 59.5 mg (0.2 mmol) of $Zn(NO_3)_2 \cdot 6H_2O$ (0.2mmol), 36.2 mg (0.2 mmol) of ATPA, and 50 mg (0.23 mmol) of L-H_2IDPA were weighed into a 20-mL scintillation vial. To the solids, 3 mL of DMF, 1 mL of EtOH, and 300 μL of water were added. The resulting yellow solution was capped and heated in an oven at 120 °C for 2 days, followed by slow cooling. Brown, bulk-like crystals were obtained and washed with DMF. Yield: 60%.

Preparation of [D-Zn_2(ATPA)(H_2IDPA)$_2$] (D-2): Under the same conditions used for the preparation of **L-2**, D-H_2IDPA was substituted for L-H_2IDPA to obtain high-quality brown bulk crystals of **D-2**.

Preparation of [L-Zn_2(DHTA)(H_2IDPA)$_2$] (L-3): 59.5 mg (0.2 mmol) of $Zn(CH_3COO)_2 \cdot 2H_2O$, 39.6 mg (0.2 mmol) of DHTA, and 50 mg (0.23 mmol) of L-H_2IDPA were weighed into a 20-mL scintillation vial. To the solids, 3 mL of DMF, 1 mL of EtOH, and 250 μL of water were added. The resulting yellow solution was capped and heated in an oven at 100 °C for 2 days, followed by slow cooling. Bright yellow, strip-like crystals were obtained and washed with DMF. Yield: 55%.

Preparation of [D--Zn_2(DHTA) (H_2IDPA)$_2$] (D-3): Under the same conditions used for the preparation of **L-3**, D-H_2IDPA was substituted for L-H_2IDPA to obtain high-quality, bright yellow, strip-like crystals of **D-3**.

2.4. Crystal structure and characterization

Table S1. Crystal Data and Structure Refinement for **L-1**, **L-2**, and **L-3**.

Compound	**L-1**	**L-2**	**L-3**
CCDC number	2415207	2415211	2415208
Empirical formula	$C_{26}H_{26}N_4O_{12}Zn_2$	$C_{26}H_{28}N_5O_{12}Zn_2$	$C_{26}H_{26}N_4O_{14}Zn_2$
Formula weight	717.25	733.26	749.25

Crystal system	orthorhombic	orthorhombic	monoclinic
Space group	$P2_12_12$	$P2_12_12$	$P2_1$
a/Å	8.58480(10)	11.38010(10)	8.54460(10)
b/Å	11.35440(10)	8.56240(10)	11.37800(10)
c/Å	14.3440(2)	14.65340(10)	14.95310(10)
α/°	90	90	90
β/°	90	90	92.0730(10)
γ/°	90	90	90
Volume/Å^3	1395.18(3)	1427.84(2)	1452.80(2)
Z	2	2	2
Flack parameter	-0.02(3)	0.41(13)	0.49(7)

Table S2. Crystal Data and Structure Refinement for **D-1**, **D-2**, and **D-3**.

Compound	**D-1**	**D-2**	**D-3**
CCDC	2415209	2415210	2415212
Empirical formula	$C_{26}H_{24}N_4O_{12}Zn_2$	$C_{26}H_{28}N_5O_{12}Zn_2$	$C_{26}H_{26}N_4O_{14}Zn_2$
Formula weight	715.23	733.27	1482.37
Crystal system	orthorhombic	orthorhombic	monoclinic
Space group	$P2_12_12$	$P2_12_12$	$P2_1$
a/Å	8.5952(2)	8.50770(10)	8.52060(10)
b/Å	11.3099(2)	11.3704(2)	11.3910(2)
c/Å	14.1931(3)	14.5983(2)	15.0356(3)
α/°	90	90	90
β/°	90	90	92.1560(10)
γ/°	90	90	90
Volume/Å3	1379.72(5)	1412.18(4)	1458.29(4)
Z	2	2	2
Flack parameter	0.09(3)	0.28(9)	0.07(8)

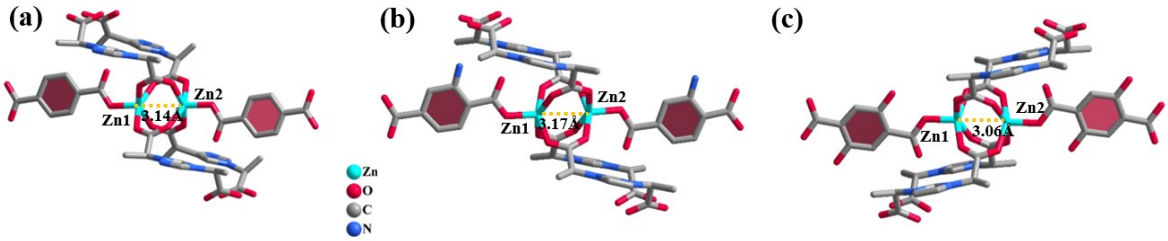

Figure S8. The asymmetric units of **L-1**, **L-2**, and **L-3**.

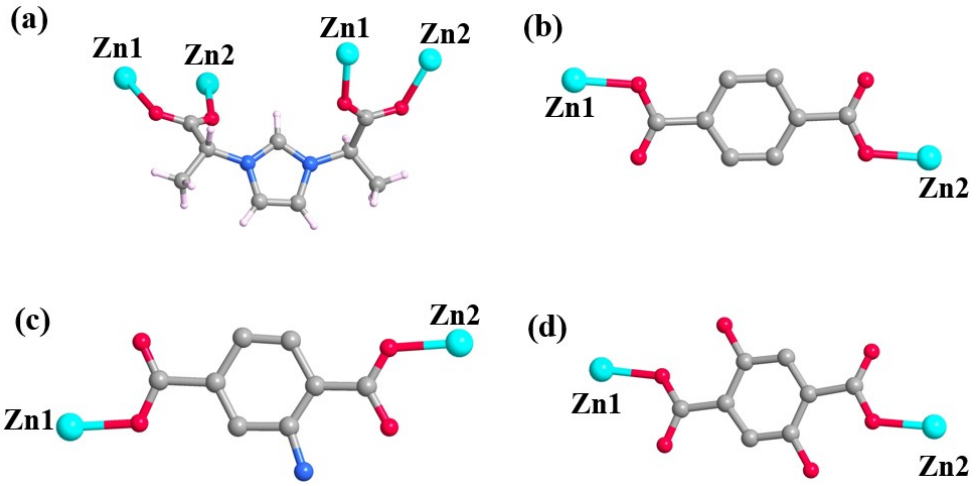

Figure S9. The coordination environment of L-H_2IDPA, TPA, ATPA, and DHTA ligand molecules.

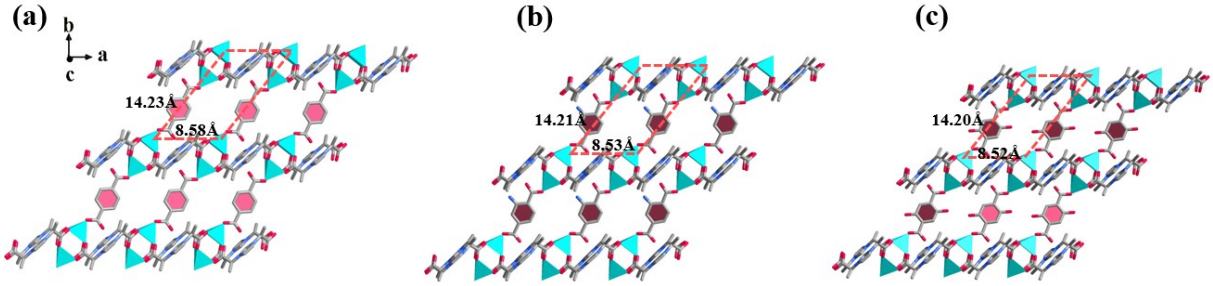

Figure S10. The 2D layered structure of **L-1**, **L-2**, and **L-3**.

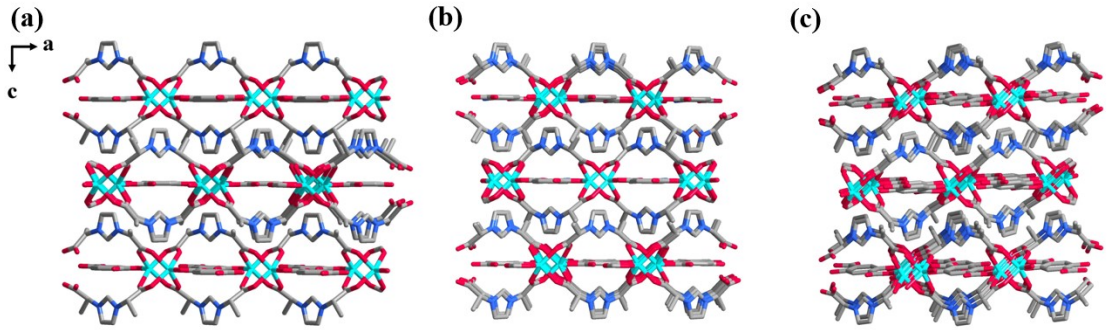

Figure S11. The 3D stacking diagrams for **L-1**, **L-2**, and **L-3** along the b-axis.

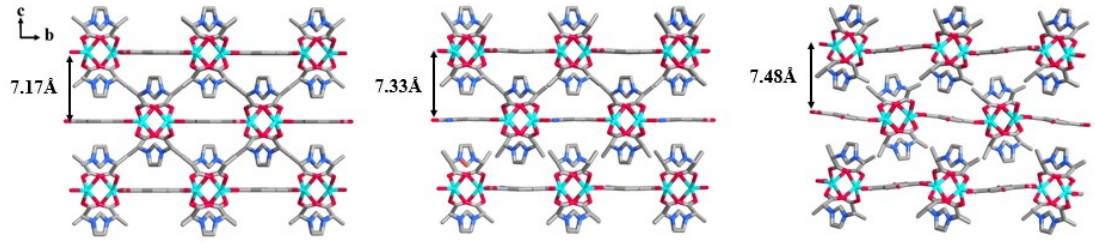

Figure S12. The 3D stacking diagrams for **L-1**, **L-2**, and **L-3** along the a-axis, with layer spacing of 7.17Å, 7.33 Å and 7.48 Å, respectively.

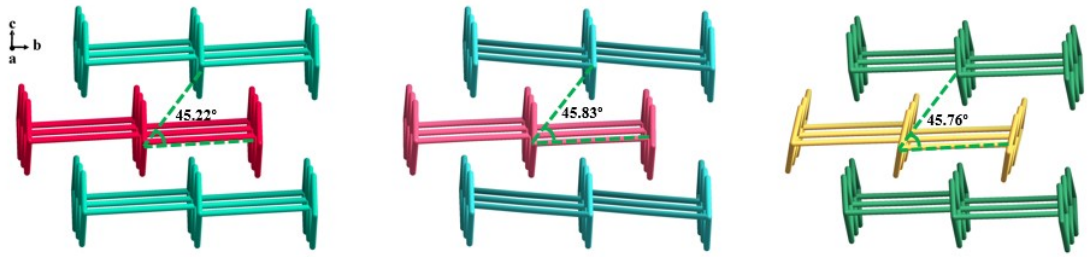

Figure S13. The topos diagram of **L-1**, **L-2**, and **L-3** along the a-axis. The angles between layers are 45.22°, 45.83°, and 45.76°, respectively.

2.5 The fundamental characterization of compounds.

2.5.1 Crystal purity analysis spectra.

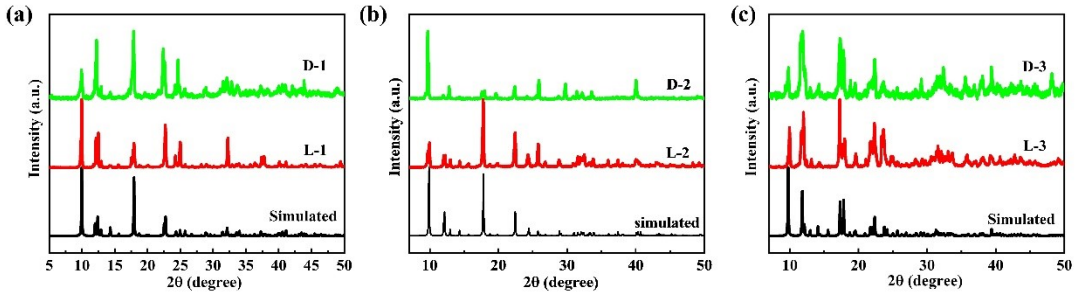

Figure S14. Simulated and measured PXRD patterns of (a) **L/D-1**, (b) **L-/D-2**, and (c) **L/D-3.**

2.5.1 Solvent and pH stability spectra.

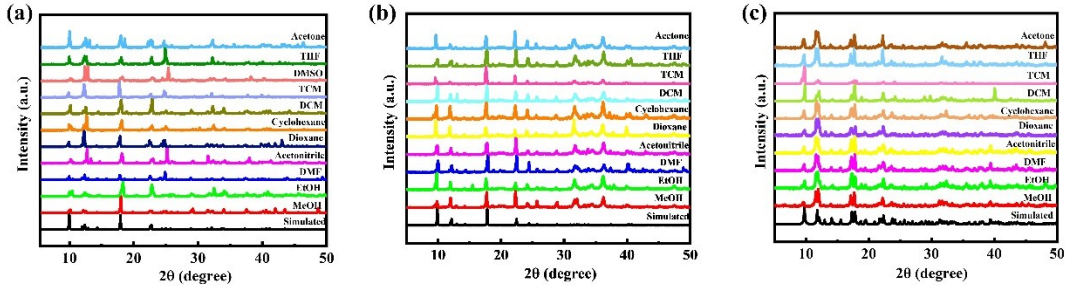

Figure S15. PXRD pattern of **L-1**, **L-2** and **L-3** soaked in 4 ml of 11 commonly used solvents for 7 days.

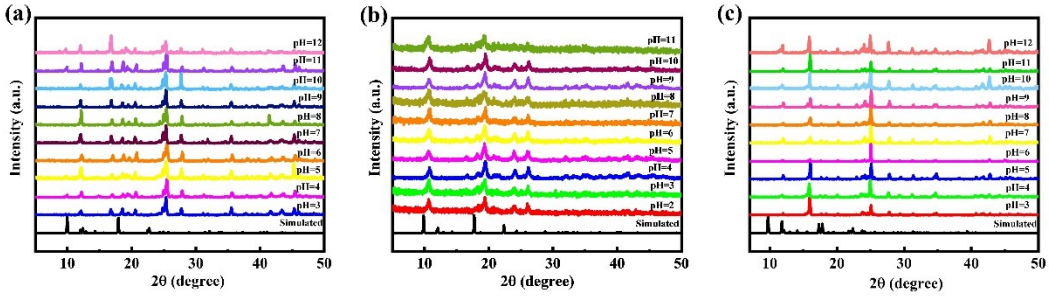

Figure S16. PXRD pattern of **L-1**, **L-2** and **L-3** soaked in aqueous solution with pH= 2~12 for 1 day.

2.5.2 Thermogravimetric analysis spectra.

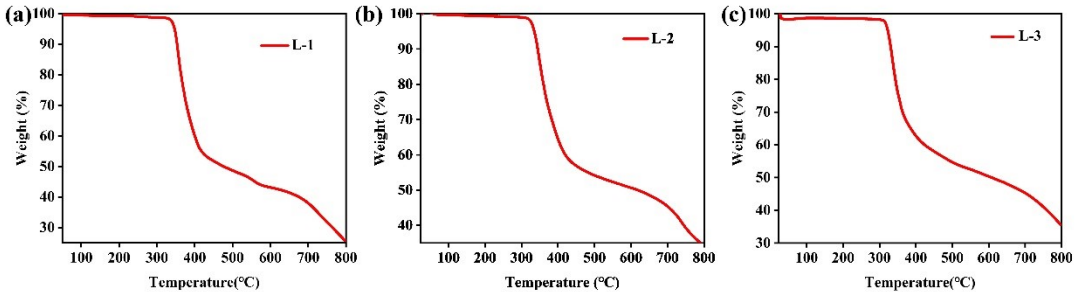

Figure S17. Thermal stability of L-1, L-2, and L-3 in the range of 24 to 800 °C.

2.6 The luminous properties of the compound

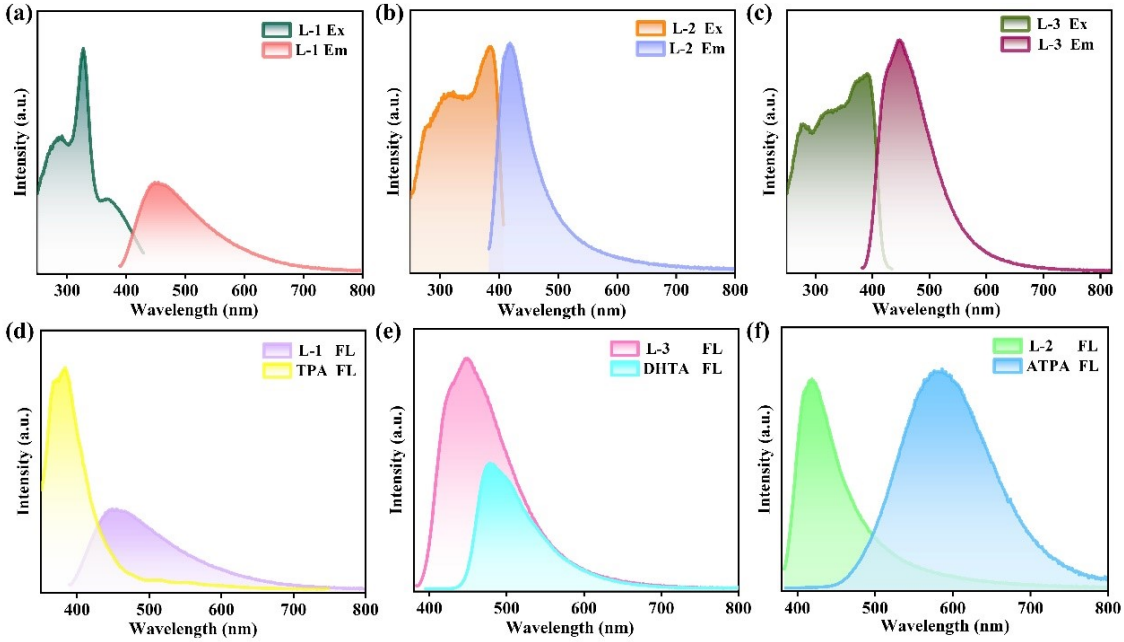

Figure S18. The excitation and emission spectra of **L-1**, **L-2**, and **L-3** are shown in (a, (b) and (c), respectively. (d), (e) and (f) are the fluorescence spectra of **L-1**, **L-2**, **L-3** and their luminescent ligands, respectively.

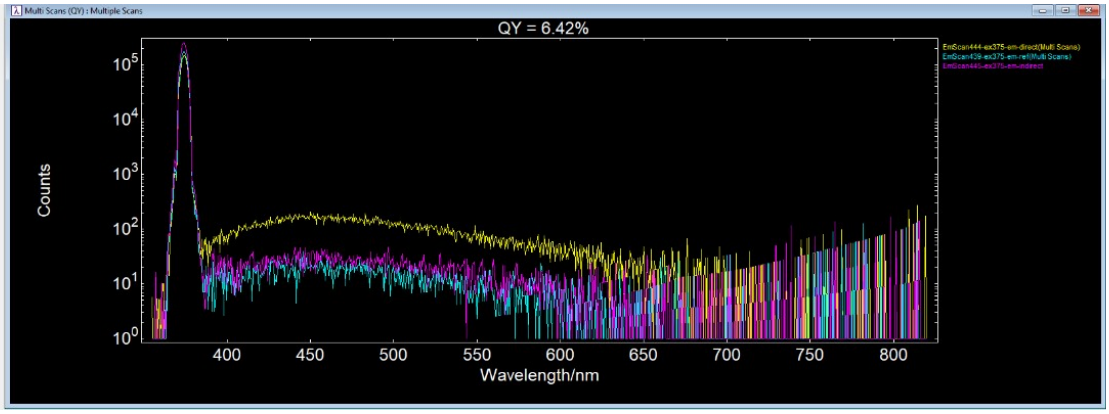

Figure S19. Quantum yield diagram of **L-1**.

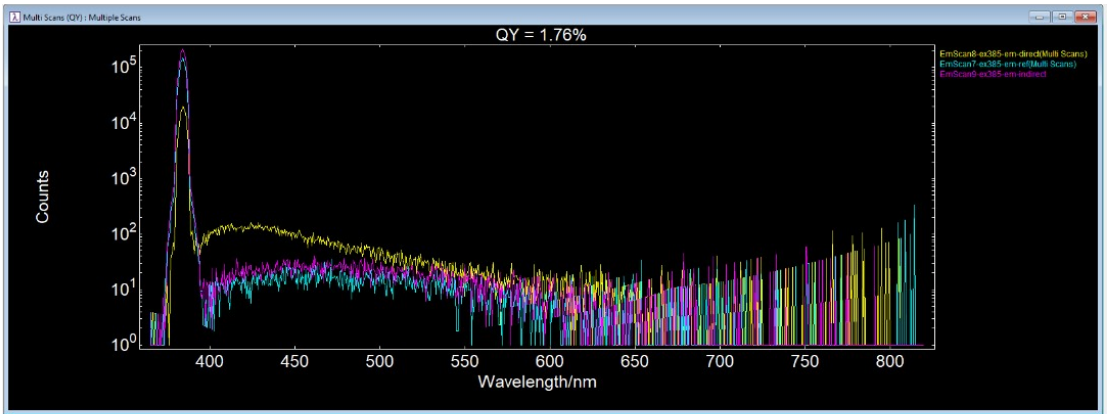

Figure S20. Quantum yield diagram of **L-2**.

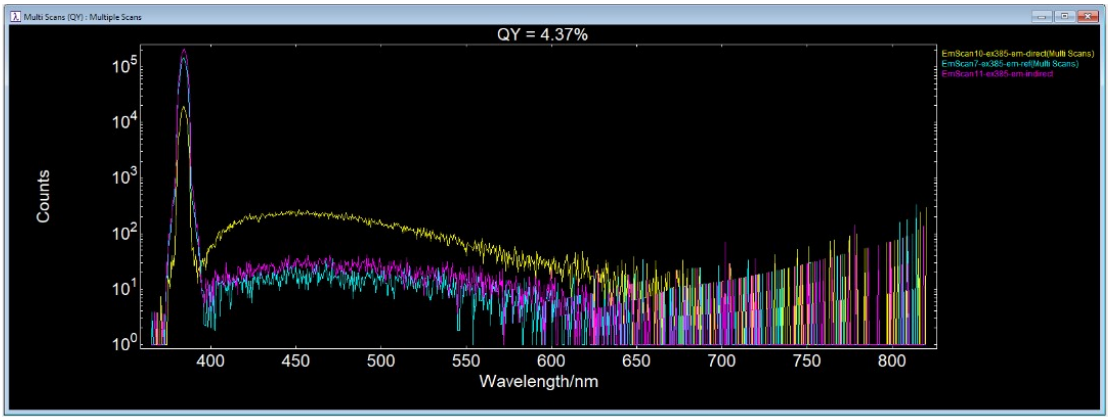

Figure S21. Quantum yield diagram of **L-3**.

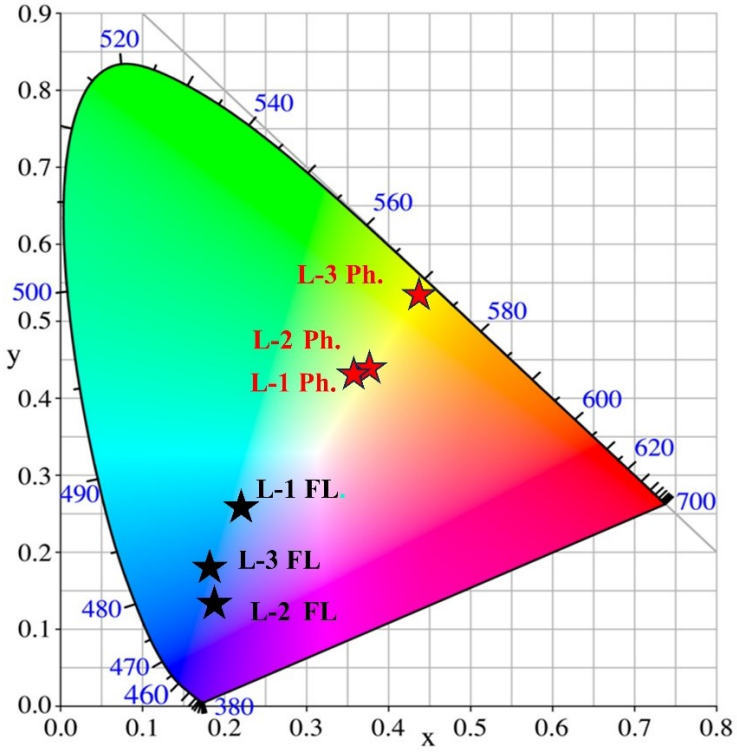

Figure S22. CIE coordinates of fluorescence and phosphorescence of **L-1**, **L-2**, and **L-3** crystals.

Table S3. CMOFs with high g_{lum} value.

Compound(s)	Metal Center	Main Ligand(s)	g_{lum}	Quantum Yield	Ref.
$[Zn_2Cam_2DAP]_n$	Zn^{2+}	chiral camphoric acid 2,7-diazapyrene ligand	3×10^{-3} -8×10^{-3}		3
DCF-17/LCF-17 DCF-18/LCF-18	Cd^{2+}	D/L-cam tetra(3-imidazoylphenyl) ethylene pyridinyl)phenyl][1,1':2',1"-terphenyl]-4,4"-diyl]bis[pyridine]	$\pm 1.0\times10^{-2}$ $\pm 9.2\times10^{-3}$		4
$[Zn_2(R/S\text{-}L)(H_2O)_3](NO_3)_2\}_n$	Zn^{2+}	2-hydroxy-4-(pyridin-4-yl)benzaldehyde (HPB) chiral1,2-diaminocyclohexane (R/S-DCH)	$\pm3.5\times10^{-3}$	8.4%	5
L-/D-ZIF	Zn^{2+}	L-His and Hmim、TEA、(Package achiral dyes, QDs, and UCNPs)	-4.3×10^{-3} 5.0×10^{-3} $\pm1:2\times10^{-2}$		6
Zn-L1 and Zn-L2 colloids	Zn^{2+}	L1、L2	0.05 和 0.03	3–4% 40–83%	7
Cd(D-MA)(BIP) (DCF-13) Cd(L-MA)(BIP) (LCF-13)	Cd^{2+}	2,6-bis(1-imidazoly)pyridine (BIP) D/L-Malic acid (D/L-MA)	$\pm5.0\times10^{-3}$	7.35%	8
Cd_2(D/L-Cam)$_2$(TPyPE) Zn_2(D/L-Cam)$_2$(TPyPE)	Cd^{2+}/Zn^{2+}	D/L-Cam =D/L-camphoric acid, TPyPE = 4,4',4'',4'''-(1,2-henediidenetetra-4,1-phenylene)tetrakis[pyridine]) w	4.9×10^{-3} 1.3×10^{-3}	40.79% 45.40%	9
L-/D-MOF	Cd^{2+}	tetrakis(4-pyridylphenyl)ethylene (TPyPE) camphoric acid (Cam)	-1.2×10^{-2}		10
R/S-ZnIDC R/S-ZnIDC(bpy)	Zn^{2+}	IDC =1H-Imidazole-4,5-dicarboxylate	$\pm5.2\times10^{-3}$ $\pm3.7\times10^{-2}$		11

R/S-ZnIDC(bpe)		bpy = 4,4′-Bipyridine bpe =trans-1,2-Bis(4-pyridyl) ethylene)	$\pm 7.2\times10^{-3}$		
P/M-Et **P/M-Et (Cd)**	Zn^{2+} Cd^{2+}	2-ethyl-5-methyl-1H-imidazole-4-carbaldehyde 1,2-diaminocyclohexane	0.015	47.3%	[12]
L-/DCF-10	Zn^{2+}	1H-1,2,3-triazolopyridine (Trzpy) D/L-alanine	1.8×0^{-3} 2.4×10^{-3}	9.88%	[13]

2.7 Detailed Description of Crystal Application Preparation

Preparation of "lock" pattern molds and pretreatment of crystals and ligands:

In the preparation process of the anti-counterfeiting "lock", the mold of the "lock" pattern was purchased by us online. Before the formal pattern production, we have fully ground the crystal and ligand materials in a mortar. This step aims to refine the crystals and ligands to a uniform powder state. This not only facilitates the presentation of a more aesthetically pleasing and smooth visual effect in the fabricated patterns but also demonstrates superior photoluminescence performance, laying a solid foundation for the anti-counterfeiting features of the anti-counterfeiting lock. All the patterns were photographed in the dark environment at room temperature to eliminate the interference of external light to the greatest extent and ensure the authenticity and clarity of the pattern features recorded.

The letters "O" and "K" preparation and potential applications in electronic device:

The molds for the letters "O" and "K" are fabricated using 3D printing technology. In the process of exciting the crystal to emit light, the ultraviolet lamp must be ensured to directly illuminate the crystal surface. The polarized light we observe from the crystal is the luminescence state of the crystal after it has been filtered by the polarizer. The purpose of this operation detail is: on the one hand, to ensure that the captured crystal luminescence photo is true polarized light information, effectively avoiding the interference of non-polarized light; On the other hand, through the enhancement and attenuation phenomena of polarized light, the changes in the chiral luminescence characteristics of the crystal can be observed more intuitively and clearly, further enhancing the anti-counterfeiting strength and reliability of the anti-counterfeiting lock.

Based on the unique chiral optical properties exhibited by the crystal, we have

conceived a simple logic electronic device solution with potential application value. However, it should be noted that at the current stage, we have only verified the feasibility framework of this device from the theoretical level and have not yet completed its physical manufacturing and functional verification.

3. References

1. X. Wang, Z. Wang, Z. Wang, T.-F. Liu, S. Li, F. Wang and J. Zhang, Synthesis of Homochiral N-Heterocyclic Carbene-Based Nanosheets for Enhanced Asymmetric Catalysis, *Adv. Sci.*, 2024, **12**, 2412592.
2. H. R. Zheng, Q. Q. Wang, X. C. Wang, F. Wang, S. Li and J. Zhang, Dual-ligand chiral MOFs exhibiting circularly polarized room temperature phosphorescence for anti-counterfeiting, *Sci. China. Chem.*, 2025, DOI: 10.1007/s11426-024-2442-0, DOI: 10.1007/s11426-11024-12442-11420.
3. S.-M. Chen, L.-M. Chang, X.-K. Yang, T. Luo, H. Xu, Z.-G. Gu and J. Zhang, Liquid-Phase Epitaxial Growth of Azapyrene-Based Chiral Metal-Organic Framework Thin Films for Circularly Polarized Luminescence, *ACS Appl. Mater. Interfaces.*, 2019, **11**, 31421-31426.
4. H. R. Fu, D. D. Ren, K. Zhang, H. Chen, X. Lu, Q. R. Ding and L. F. Ma, Induced Absolute Configuration of Achiral Tetradentate Ligands in Metal-Organic Frameworks for Circularly Polarized Luminescence, *Chin. J. Chem.*, 2024, **42**, 1260-1266.
5. X. Z. Wang, Y. T. Liu, C. Zhou, B. Wang, D. Luo, M. Xie, M.-Y. Sun, Y.-L. Huang, J. Luo, Y. Wu, S. Zhang, X.-P. Zhou and D. Li, Amplified circularly polarized luminescence of chiral metal-organic frameworks via post-synthetic installing pillars, *Chin. Chem. Lett.*, 2024, **35**, 109380.
6. T. Zhao, J. Han, X. Jin, M. Zhou, Y. Liu, P. Duan and M. Liu, Dual-Mode Induction of Tunable Circularly Polarized Luminescence from Chiral Metal-Organic Frameworks, *Research.*, 2020, **2020**, 6452123.
7. J. C. Huang, G. M. Ye, M. Yu, R. Huang, Z. Zhao, A. Qin, S. T. Wu and Z. Xie, Circularly Polarized Luminescence of Achiral Metal-Organic Colloids and Guest Molecules in a Vortex Field, *Chem. Eur. J.*, 2021, **27**, 6760-6766.
8. H. R. Fu, R. Y. Zhang, D. D. Ren, K. Zhang, J. Yuan, X. Y. Lu and Q. R. Ding, Chiral Coordination Assembly-Induced Phosphorescent Frameworks for Circularly Polarized Phosphorescence, *Cryst. Growth. Des.*, 2024, **24**, 4819-4824.
9. H. Q. Yin, J. Chen, Y. W. Xue, J. Ren, X. H. Wang, H. R. Fan, S. Y. Wei, B. Sun and Z. M. Zhang, Loading Dyes into Chiral Cd/Zn-Metal-Organic Frameworks for Efficient Full-Color Circularly Polarized Luminescence, *Angew. Chem. Int. Ed.*, 2024, **163**, e202407596.
10. W. Shang, X. Zhu, T. Liang, C. Du, L. Hu, T. Li and M. Liu, Chiral Reticular Self-Assembly of Achiral AIEgen into Optically Pure Metal-Organic Frameworks (MOFs) with Dual Mechano-Switchable Circularly Polarized Luminescence, *Angew. Chem. Int. Ed.*, 2020, **59**, 12811-12816.
11. M. Y. Zheng, Z. B. Jin, Z. Z. Ma, Z. G. Gu and J. Zhang, Photo-Curable 3D Printing of Circularly Polarized Afterglow Metal-Organic Framework Monoliths, *Adv. Mater.*, 2024, **36**, 2313749
12. X. Z. Wang, C. W. Zhou, J. Zheng, Z. X. Lian, M. Y. Sun, Y. L. Huang, D. Luo, Y. Y. Li and X. P. Zhou, Highly Boosting Circularly Polarized Luminescence of Chiral Metal-Imidazolate Frameworks, *Adv. Sci.*, 2023, **10**, 2207333.
13. H. Liu, D. D. Ren, P. F. Gao, K. Zhang, Y. P. Wu, H. R. Fu and L. F. Ma, Multicolor-tunable room-temperature afterglow and circularly polarized luminescence in chirality-induced coordination assemblies, *Chem. Sci.*, 2022, **13**, 13922-13929.